

Laser cooling transitions in atomic erbium

H. Y. Ban,* M. Jacka,[†] J. L. Hanssen, J. Reader and J. J. McClelland

Physics Laboratory
National Institute of Standards and Technology
Gaithersburg, MD 20899

*present address: Department of Physics and Astronomy, University of Pennsylvania, Philadelphia, PA

[†]permanent address: Department of Physics, York University, York, UK
jabez.mcclelland@nist.gov

Abstract We discuss laser cooling opportunities in atomic erbium, identifying five $J \rightarrow J + 1$ transitions from the $4f^{12}6s^2\ ^3H_6$ ground state that are accessible to common visible and near-infrared continuous-wave tunable lasers. We present lifetime measurements for the $4f^{11}(^4I_{15/2}^o)5d_{5/2}6s^2(15/2, 5/2)_7^o$ state at 11888 cm^{-1} and the $4f^{11}(^4I_{13/2}^o)5d_{3/2}6s^2(13/2, 5/2)_7^o$ state at 15847 cm^{-1} , showing values of $20 \pm 4\ \mu\text{s}$ and $5.6 \pm 1.4\ \mu\text{s}$, respectively. We also present a calculated value of $13 \pm 7\ \text{s}^{-1}$ for the transition rate from the $4f^{11}(^4I_{15/2}^o)5d_{3/2}6s^2(15/2, 3/2)_7^o$ state at 7697 cm^{-1} to the ground state, based on scaled Hartree-Fock energy parameters. Laser cooling on these transitions in combination with a strong, fast (5.8 ns) laser cooling transition at 401 nm, suggest new opportunities for narrowband laser cooling of a large-magnetic moment atom, with possible applications in quantum information processing, high-precision atomic clocks, quantum degenerate gases, and deterministic single-atom doping of materials.

OCIS Codes: (020.7010) Trapping; (020.4900) Oscillator strengths

References and links

1. C. Y. Chen, Y. M. Li, K. Bailey, T. P. O'Connor, L. Young, and Z.-T. Lu, "Ultrasensitive isotope trace analyses with a magneto-optical trap," *Science* **286**, 1139-1141 (1999).
2. J. Helmcke, G. Wilpers, T. Binnewies, C. Degenhardt, U. Sterr, H. Schnatz, and F. Riehle, "Optical frequency standard based on cold Ca atoms," *IEEE Trans. Instr. Meas.*, **52**, 250-254 (2003).
3. J. R. Anglin and W. Ketterle, "Bose-Einstein condensation of atomic gases," *Nature* **416**, 211-218 (2002).
4. C. Monroe, "Quantum information processing with atoms and photons," *Nature* **416**, 238-246 (2002).
5. J. J. McClelland, "Nanofabrication via Atom Optics," in *Handbook of Nanostructured Materials and Nanotechnology*, ed. by H. S. Nalwa, vol. I, (Academic Press, San Diego, CA, 2000), p. 335-385. D. Meschede and H. Metcalf, "Atomic nanofabrication: atomic deposition and lithography by laser and magnetic forces," *J. Phys. D – Appl. Phys.* **36**, R17-R38 (2003).
6. W. R. Anderson, C. C. Bradley, J. J. McClelland, and R. J. Celotta, "Minimizing feature width in atom-optically fabricated chromium nanostructures," *Phys. Rev. A* **59**, 2476-2485 (1999).
7. M. Baranov, L. Dobrek, K. Góral, L. Santos, and M. Lewenstein, "Ultracold dipolar gases – a challenge for experiment and theory," *Physica Scripta*, **T102**, 74-81 (2002).
8. A. Derevianko and C. C. Cannon, "Quantum computing with magnetically interacting atoms," *Phys. Rev. A* **70**, 062319-1 – 062319-6 (2004).
9. Courtillot, A. Quessada, R. P. Kovacich, A. Bruschi, D. Kolker, J.-J. Zondy, G. D. Rovera, and P. Lemonde, "Clock transition for a future optical frequency standard with trapped atoms," *Phys. Rev. A* **68**, 030501-1 – 030501-4 (2003).
10. S. B. Hill and J. J. McClelland, "Atoms on demand: fast, deterministic production of single Cr atoms," *Appl. Phys. Lett.* **82**, 3128-3130 (2003).
11. T. Binnewies, G. Wilpers, U. Sterr, F. Riehle, J. Helmcke, T. E. Mehlstäubler, E.M. Rasel, and W. Ertmer, "Doppler Cooling and Trapping on Forbidden Transitions," *Phys. Rev. Lett.* **87**, 123002-1 – 123002-4 (2001).
12. E. A. Curtis, C. W. Oates, and L. Hollberg, "Quenched narrow-line second- and third-stage laser cooling of ^{40}Ca ," *J. Opt. Soc. Am B* **20**, 977-984 (2003).
13. U. Sterr, T. Binnewies, C. Degenhardt, G. Wilpers, J. Helmcke, and F. Riehle, "Prospects of Doppler cooling on forbidden lines," *J. Opt. Soc. Am B* **20**, 985-983 (2003).

14. H. Katori, T. Ido, Y. Isoya, and M. Kuwata-Gonokami, "Magneto-optical trapping and cooling of strontium atoms down to the photon recoil temperature," *Phys. Rev. Lett.* **82**, 1116-1119 (1999).
15. I. Courtillot, A. Quessada, R. P. Kovacich, J-J. Zondy, A. Landragin, A. Clairon, and P. Lemonde, "Efficient cooling and trapping of strontium atoms," *Opt. Lett.* **28**, 468-470 (2003).
16. S. B. Nagel, C. E. Simien, S. Laha, P. Gupta, V. S. Ashoka, and T. C. Killian, "Magnetic trapping of metastable 3P2 atomic strontium," *Phys. Rev. A* **67**, 011401-1 – 011401-4 (2003).
17. X. Xu, T. H. Loftus, J. L. Hall, A. Gallagher, and J. Ye, "Cooling and trapping of atomic strontium," *J. Opt. Soc. Am. B* **20**, 968-976 (2003).
18. T. Kuwamoto, K. Honda, Y. Takahashi, and T. Yabuzaki, "Magneto-optical trapping of Yb atoms using and intercombination line," *Phys. Rev. A* **60**, R745-R748 (1999).
19. R. Maruyana, R. H. Wynar, M. V. Romalis, A. Andalkar, M. D. Swallows, C. E. Pearson, and E. N. Forston, "Investigation of sub-Doppler cooling in an ytterbium magneto-optical trap," *Phys. Rev. A* **68**, 011403-1 – 011403-4 (2003).
20. W. C. Martin, R. Zalubas, and L. Hagan, "Atomic energy levels – the rare earth elements," NSRDS-NBS **60** (1978).
21. N. Spector, " $4f^{12}(^3H_6)6s6p$ levels of neutral erbium (Er I)," *J. Opt. Soc. Am.* **57**, 308-311 (1967).
22. H. J. Metcalf and P. van der Straten, *Laser Cooling and Trapping*, (Springer, New York, 1999).
23. J. E. Sansonetti and W. C. Martin, "Handbook of basic atomic spectroscopic data," <http://physics.nist.gov/PhysRefData/Handbook/Tables/erbiumtable3.htm>.
24. Unless otherwise noted, all uncertainty estimates in this paper are intended to be interpreted as one-standard deviation combined standard uncertainty.
25. R. J. Lipert and S. C. Lee, "Isotope shifts and hyperfine structure of erbium, dysprosium, and gadolinium by atomic-beam diode laser spectroscopy," *Appl. Phys. B* **57**, 373-379 (1993).
26. For the 841 nm line the "on" time was 200 μ s and the "off" time was 150 μ s. For the 631 nm line these values were both 100 μ s.
27. J. J. McClelland, "Optical state preparation of atoms," in *Atomic, Molecular, and Optical Physics: Atoms and Molecules*, ed. by F. B. Dunning and R. G. Hulet (Academic Press, San Diego, CA, 1995), pp. 145-170.
28. R. D. Cowan, *The theory of atomic structure and spectra*, (University of California Press, Berkeley, CA, 1981), and Cowan programs RCN, RCN2, and RCG.

1. Introduction

Over the past two decades, laser cooling of atoms has become an extremely widespread and diverse area of research. While by far the most work has been done with alkali atoms such as sodium, rubidium and cesium, there has also been an increasing interest in extending the techniques to other atoms. Fueled by the continuing introduction of new tunable laser sources and efficient wavelength doubling techniques, an ever-increasing selection of atoms has become available. These new atoms have opened new possibilities for uses of laser cooling techniques, impacting such diverse areas as trace atom detection [1], ultra-precise frequency standards [2], quantum degenerate gases [3], quantum information processing, [4], and fabrication of nanostructures [5].

As new atoms emerge as possible candidates for laser cooling – usually when a closed, or nearly-closed, laser-accessible optical transition is identified – it is useful to consider what special properties an atom may have that will enable new techniques or introduce new physics. For example, in nanostructure fabrication, the growth behavior and material properties of an atom are important [6]. In quantum degenerate gases, the ability to cool to very low temperatures, the presence of a positive scattering length, the availability of both bosonic and fermionic isotopes, and a strong dipole moment are of interest [7]. For quantum information processing, a qubit-compatible level structure and a strong ground-state magnetic moment may be of importance [8]. For ultra-precise frequency standards, extremely narrow-band laser transitions with systematic-free or characterizable frequencies provide interesting opportunities [9].

In this paper, we discuss new opportunities for laser cooling erbium atoms. As a rare-earth atom, Er has a complex energy level structure and as a result has not received much attention from the laser cooling community. Nevertheless, it has unique properties that open possibilities for a number of applications. In nanostructure fabrication, the recent development of a deterministic atom source using laser cooling techniques [10] suggests the

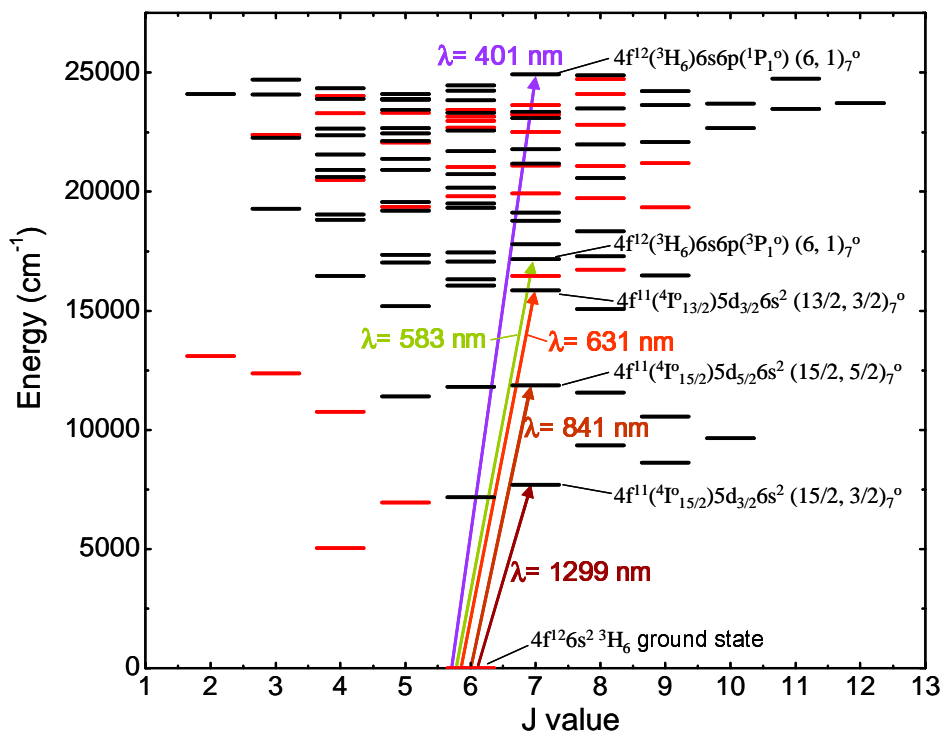


Fig. 1. Energy levels of erbium, showing five laser cooling transitions. Red horizontal lines indicate even parity states and black horizontal lines indicate odd parity states.

possibility of controlled doping of optical materials with erbium at the atom-by-atom level, which could allow fabrication of a wide range of novel photonic devices. For quantum-degenerate gas studies, Er offers very low laser cooling temperature limits as well as even and odd isotopes: ^{166}Er (34% abundance), ^{168}Er (27% abundance), ^{170}Er (15% abundance), and ^{167}Er (23% abundance, spin 7/2). For quantum information studies, Er offers a ground state with a very large magnetic moment ($7\mu_B$) for magnetic trapping, and for ultra-precise frequency standards it has several very narrowband transitions.

2. Laser cooling transitions

We have identified no less than five transitions in Er that are compatible with laser cooling, all of which originate from the ground state and are accessible to common single-frequency CW lasers. Through the measurements and calculations discussed below, we have found that among these five transitions, the lower-energy ones have very narrow natural linewidths. The possibility of laser cooling on such transitions is particularly exciting, given the recent interest in narrow-linewidth cooling on the Ca 657 nm line [11–13], the Sr 689 nm line [14–17], and the Yb 556 nm line [18,19]. In the context of these studies, Er offers the unique combination of a very large mass together with a long-wavelength cooling transition, resulting in a very low recoil limit. In addition, the large ground-state angular momentum of Er allows polarization-gradient cooling on the even isotopes.

A partial diagram of the energy levels of Er is shown in Fig. 1 [20]. The ground state is in a $4f^{12}6s^2({}^3\text{H}_6)$ configuration; that is, the parity is even and $J = 6$. Thus it is of most interest from a laser cooling perspective to consider transitions to odd parity excited states with $J = 7$. Transitions to these states will have a $J \rightarrow J + 1$ change in angular momentum, which is

necessary for a magneto-optical trap and/or polarization-gradient cooling. On examining the level diagram, we see that the four lowest-lying states of this type in Er are all accessible to common tunable lasers. The $4f^{11}(^4T_{15/2}^o)5d_{3/2}6s^2(15/2, 3/2)_7^o$ level at 7696.956 cm^{-1} can be reached with a 1299 nm diode laser, the $4f^{11}(^4T_{15/2}^o)5d_{5/2}6s^2(15/2, 5/2)_7^o$ level at 11887.503 cm^{-1} can be reached with either a diode laser or a Ti:sapphire laser operating at 841 nm, the $4f^{11}(^4T_{13/2}^o)5d_{3/2}6s^2(13/2, 3/2)_7^o$ level at 15846.549 cm^{-1} can be reached with either a diode laser or a dye laser operating at 631 nm, and the $4f^{12}(^3H_6)6s6p(^3P_1^o)(6,1)_7^o$ level at 17157.207 cm^{-1} can be reached with a dye laser operating at 583 nm. In addition to these levels, a very strong $J \rightarrow J+1$ transition to the $4f^{12}(^3H_6)6s6p(^1P_1^o)(6,1)_7^o$ level at 24943.272 cm^{-1} [21] exists which can be excited with a violet diode laser or a doubled Ti:sapphire laser operating at 401 nm. For the sake of brevity, these levels will be referred to by their laser wavelength for the remainder of this text. We also note in passing that the lowest-lying metastable level is 5000 cm^{-1} above the ground state, so its population at thermal evaporation temperatures ($1200\text{ }^\circ\text{K}$) is negligibly small at about 0.2%. Thus a thermally evaporated atomic beam will consist of essentially all ground-state atoms.

3. Transition rates

In order to analyze the laser cooling behavior of an atom, one of the most important quantities to know is the transition rate Γ for the transition on which the atom is being laser cooled. This quantity, along with the associated lifetime $\tau = 1/\Gamma$ and natural linewidth $\Delta\nu = \Gamma/2\pi$, determines a range of important quantities, such as the saturation intensity for the transition, the maximum force a laser can exert on an atom, the capture velocity for Doppler cooling, and the Doppler limit for minimum temperature [22]. Among the five possible laser cooling transitions we have identified in Er, only the 401 nm and the 583 nm transitions have rates that are available in the literature: $\Gamma = 1.7 \times 10^8\text{ s}^{-1}$ for the 401 nm transition, and $\Gamma = 1.0 \times 10^6\text{ s}^{-1}$ for the 583 nm transition [23]. Thus, a central purpose of the current study is to present rate information for the other three transitions. To accomplish this, we have carried out lifetime measurements for the upper levels of the 631 nm and 841 nm transitions, and have performed a calculation of the rate for the 1299 nm transition. These measurements and calculations will be discussed in sections 5-7 below.

4. Optical leaks

A second key property of a laser cooling transition is the possibility of optical leaks via spontaneous decay to other metastable levels instead of to the ground state. Such decay, if sufficiently fast, can interfere with laser cooling because it permits atoms to escape the continued absorption and reemission of photons necessary for efficient cooling, and can lead to loss of atoms from a cooled population.

Optical leaks can be identified by examining any energy levels below the upper level of a cooling transition and considering the selection rules for spontaneous emission. Of primary importance is spontaneous emission that is electric-dipole (E1) allowed, and hence in our case would involve even-parity states with $J = 6, 7, \text{ or } 8$. Of lesser importance, but worth checking, is the possibility of spontaneous emission via electric quadrupole (E2) or magnetic dipole (M1) transitions, which would involve odd parity levels with $J = 5$ through 9.

Of the five laser cooling transitions we have identified in Er, the lower three have, for all practical purposes, no optical leaks. Below the 1299 nm state there are only two even-parity metastable levels, but these have J values of 4 and 5, so electric dipole radiation is forbidden. Below the 841 nm state, there is one additional even-parity level, and below the 631 nm state, two more even parity levels become available. As with the 1299 nm state, however, transitions to these levels involve forbidden J values of 2, 3 or 4. In addition to these even-parity metastable levels, there are a few odd-parity levels that in principle could open leak channels. However, these either involve a forbidden value of J or are separated by so small an energy that an E2 or an M1 spontaneous transition rate would be vanishingly small. Based

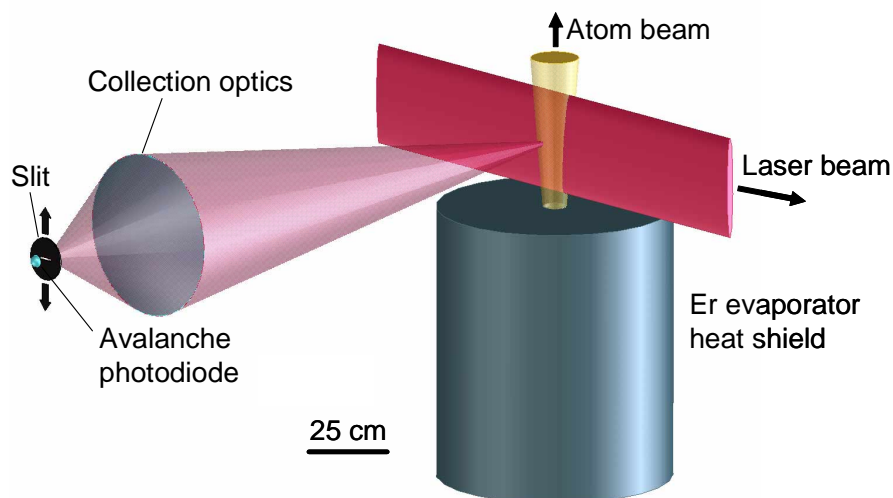


Fig. 2. Schematic of the crossed-beam experimental arrangement.

on these simple considerations, it is very unlikely that the lifetime for leaking out of any of these three laser cooling levels to a metastable state will be of any significance, and laser cooling transitions involving the ground state and these levels will be effectively closed.

The 583 nm level presents the first opportunity for leaks in which the $\Delta J = 0, \pm 1$ selection rule for electric dipole radiation is satisfied. However, transitions to the two newly accessible levels involve very small energy changes of 430 cm^{-1} and 630 cm^{-1} , and hence are expected to have very small transition rates. To support this expectation, we extracted transition rates from the calculation described in section 6 below, obtaining values of 0.017 s^{-1} and 0.0049 s^{-1} , respectively. While the accuracy of the calculation for such small transition rates cannot be guaranteed, the fact that such a negligible value is obtained is reassuring.

On examining the 401 nm level, it appears that in this case there are a number of optical leakage paths with $\Delta J = 0, \pm 1$, allowing electric-dipole spontaneous emission. All these leakage transitions involve configuration changes that are not strongly coupled with dipole radiation, however, suggesting that the net leakage should be relatively small. To get some idea of its magnitude, we extracted transition rates from the calculation described in section 6, as we did for the 583 nm level. The calculation revealed several transition rates in the 10^3 s^{-1} range, resulting in a total loss rate of $1.6 \times 10^4 \text{ s}^{-1}$. When compared to the extremely fast fluorescence decay rate of $1.7 \times 10^8 \text{ s}^{-1}$ to the ground state, this rate appears small enough to allow some degree of laser cooling to be implemented without incurring appreciable loss. However, for some applications it may prove necessary to take extra steps, such as avoiding high excited state populations or using repumping lasers, to get a large population of cooled atoms. We should also note that there may be dipole-allowed cascade pathways back to the ground state that ameliorate some of these leaks. The full impact of the leaks and possible return pathways for the 401 nm transition is difficult to evaluate with our current state of knowledge of the transition rates between all the levels involved. Future work will involve more calculations and further experimental investigations to determine these effects.

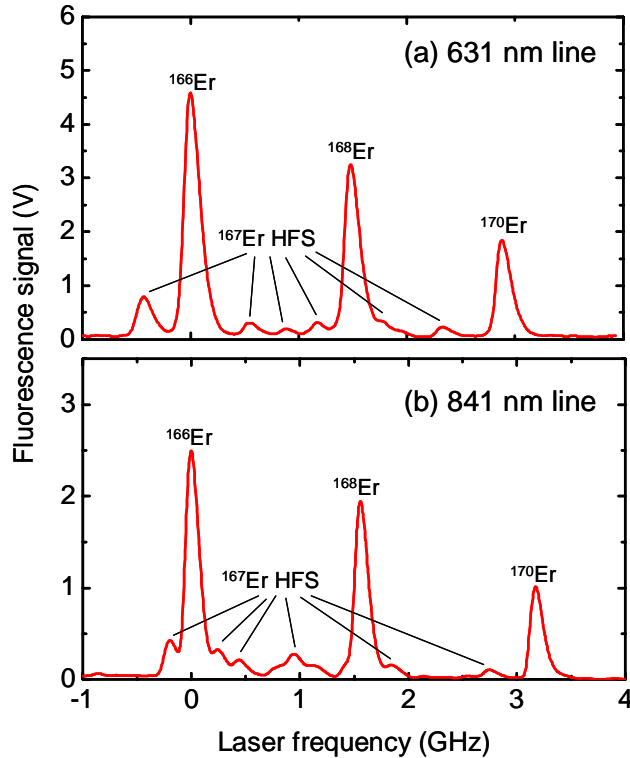


Fig. 3. Measured fluorescence spectra for (a) the 631 nm line and (b) the 841 nm line, showing the isotopes ^{166}Er , ^{168}Er and ^{170}Er , and the hyperfine structure (HFS) for ^{167}Er .

5. Experiments

Our experiments were carried out in a crossed-beam laser-induced fluorescence apparatus (see Fig. 2). A beam of Er atoms was produced in a vacuum chamber by placing a ≈ 100 mg piece of Er metal in a Ta evaporation boat heated by (39 to 45) A of current. Based on optical pyrometer measurements, and corroborated by signal size estimates, the temperature of the source was estimated to be about 1200 °K, a temperature at which Er has a vapor pressure of about 2×10^{-3} Pa (1.5×10^{-5} Torr). The source was surrounded by a Ta heat shield with a 6 mm hole located ≈ 25 mm above the boat, which provided crude collimation. Laser light was generated either with a single-frequency, stabilized Ti:sapphire laser for the 841 nm line, or with a grating-stabilized diode laser for the 631 nm line. The laser beam passed through a 200 MHz acousto-optic modulator (AOM), which switched the light on and off with measured rise and fall times of 31 ± 2 ns (10% to 90%) [24]. Before entering the vacuum chamber, the beam was expanded with a cylindrical telescope to an elliptical shape with a nominally Gaussian profile. For the 841 nm measurements, the $1/e^2$ full widths were 35 ± 1 mm along the atom beam propagation direction and 2.0 ± 0.5 mm transverse to the atom beam. For the 631 nm measurements, these values were 22 ± 1 mm and 1.2 ± 0.5 mm, respectively. In each case the beam was truncated by a 26 mm-diameter aperture just before entering the vacuum chamber, where it intersected the atom beam approximately 30 mm above the source. The laser powers were 80 ± 5 mW for the 841 nm line, and 0.8 ± 0.1 mW for the 631 nm line, resulting in peak intensities of 2900 W/m^2 and 72 W/m^2 , respectively.

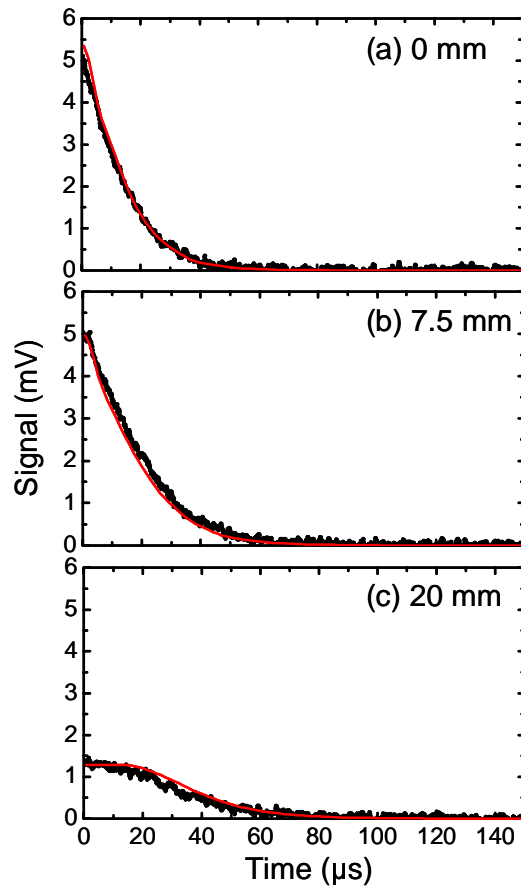


Fig. 4. 841 nm fluorescence decay at three detector positions relative to the laser-atom beam intersection. (a) 0 mm, (b) 7.5 mm, and (c) 20 mm. Black dots indicate measurements, and red line indicates model used to extract lifetime. Extracted lifetime is $20 \pm 4 \mu\text{s}$.

Fluorescence was collected by an $f/1.2$, 50 mm-focal-length camera lens positioned 140 ± 5 mm from the laser-atom beam intersection. After passing through an appropriate interference filter, the light was imaged with magnification 0.4x onto a $0.2 \text{ mm} \times 3 \text{ mm}$ slit with long dimension oriented perpendicular to the atom beam direction. The imaging system was carefully aligned to avoid detection of stray scattered light, which at 841 nm had a strong component from the erbium evaporator despite the interference filter. Light passing through the slit was detected with a large-area (3 mm diameter) avalanche photodiode and the resulting signal was recorded with a lock-in amplifier and/or an oscilloscope. The electronic rise and fall times of the detection system were measured to be no greater than $1 \mu\text{s}$.

Fig. 3 shows typical laser-induced fluorescence spectra obtained by using the AOM to modulate the laser light at 2.9 kHz (841 nm line) or 5 kHz (631 nm line), and detecting the signal with the lock-in amplifier. The lock-in time constant was set to 10 ms, the output filter was set to 12 db per octave, and the signal was recorded in an oscilloscope while the laser frequency was scanned at 3.8 GHz s^{-1} (841 nm line) or 5.3 GHz s^{-1} (631 nm line), averaging over 128 sweeps for the final result. Clearly visible in the spectra are the single lines from the three even isotopes ^{166}Er , ^{168}Er , and ^{170}Er , and the hyperfine structure of the odd isotope ^{167}Er .

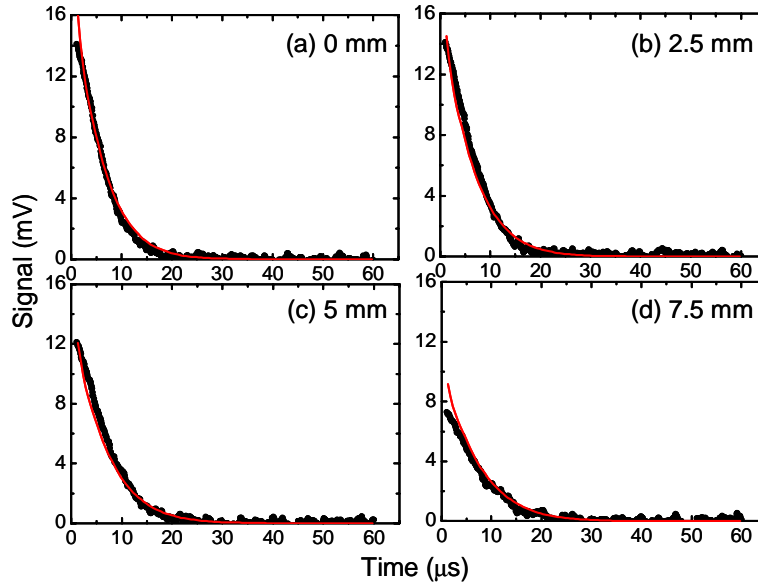


Fig. 5. 631 nm fluorescence decay at three detector positions relative to the laser-atom beam intersection. (a) 0 mm, (b) 2.5 mm, (c) 5 mm, and (d) 7.5 mm. Black dots indicate measurements, and red line indicates model used to extract lifetime. Extracted lifetime is $5.6 \pm 1.4 \mu\text{s}$.

We note that the spectrum of the 841 nm line is in good agreement with previous measurements in the literature [25].

Lifetime measurements were carried out by chopping the laser light with the AOM [26] and recording the decay of the fluorescence signal from the largest (i.e., ^{166}Er) peak with the oscilloscope, averaging over typically 2048 cycles. While in some situations such a measurement can be straightforward, in our case interpretation was complicated by the fact that, with the long fluorescent lifetimes involved, excited atoms can fly out of the observation region before they decay. Clear evidence of this effect was found in both a visibly non-exponential decay in the fluorescence, and a marked variation in decay lifetimes for different locations along the atom beam, if an exponential decay was forced to fit the data.

In order to extract meaningful lifetimes from our measurements, we conducted a series of decay measurements at different locations along the atom beam and developed a model for the expected decay at each location based on averaging over velocity and angular distributions. Using measurements of the laser beam profile and intensity, we numerically integrated a two-level rate equation to derive the time evolution of the excited state fraction, given that an atom is exposed to a light intensity that is time dependent as a result of its traveling at a certain velocity on a certain trajectory through the spatially varying light field. A rate equation model was used instead of an optical Bloch equation model to reduce computation time, and was considered adequate because any coherence effects would be lost in the velocity and angle averaging. Detuning, as introduced by the Doppler shift for atoms traveling at a small angle relative to the laser beam, was found to play a significant role in this model, and was included via an *ad hoc* Lorentzian factor [27].

The rate equation model allowed us to calculate the fluorescence signal at a given detector position as a function of time, with velocity and trajectory angle as parameters. Averaging over a Maxwell-Boltzmann speed distribution with most probable velocity 350 m s^{-1} (based on the estimated source temperature), and an angular distribution derived from the detector

slit size and distance from the source, then allowed us to calculate a decay that mimicked the experimental observations at a given detector position.

Using the model, decay curves were calculated at each of the detector positions where measurements were conducted, and a least-squares fit was conducted with three free parameters: the lifetime, a normalization constant, and an offset for the detector position, which was necessary because it was difficult to determine the absolute detector position relative to the laser beam center. To conduct the fit, the total χ^2 for all of the detector positions combined was minimized for a single set of parameters, and the minimization was carried out by recalculating and reaveraging a complete set of trajectories every time a new set of parameters was sampled. Once an optimum fit was obtained, the uncertainty in the lifetime was derived by stepping the lifetime through a series of values around the optimum while allowing the other two parameters to re-minimize χ^2 at each value. The lifetime values for which χ^2 is doubled on either side of the minimum provide an estimate for a one-standard-deviation uncertainty in the lifetime. Uncertainty resulting from inaccurate estimates of experimental parameters such as Er source temperature, laser beam profiles, and imaging magnification was examined by conducting additional minimizations with variations in these parameters. In all cases the observed lifetime variations were far smaller than the one-standard deviation uncertainty obtained as described above.

Fig. 4 shows the measured fluorescence decays and best fit models for the 841 nm line, where three nominal detector positions were sampled: 0 mm, 7.5 mm and 20 mm, as measured in the direction of atom beam propagation from the approximate center of the laser beam. We note that in the fitting process, these detector positions required correction by an offset of 2.5 mm. Based on these measurements, the best-fit lifetime was found to be 20 ± 4 μ s. Fig. 5 shows similar results for the 631 nm line, where measurements were conducted at 0 mm, 2.5 mm, 5 mm, and 7.5 mm (these values required an offset correction of 3.5 mm during the fitting). The result of this set of measurements is a lifetime of 5.6 ± 1.4 μ s.

6. Calculations

In order to estimate the transition rate of the 1299 nm line, we carried out calculations of the atomic structure of Er I with the relativistic Hartree-Fock code of Cowan [28]. The calculation included the even configuration $4f^{12}6s^2$ and the interacting odd configurations $4f^{11}5d6s^2$, $4f^{12}6s6p$, $4f^{11}5d^26s$, and $4f^{11}5d^3$. We used a scale factor of 0.80 for the direct and exchange internal electrostatic interactions, 1.00 for the internal spin-orbit interactions, and 0.90 for the configuration interactions. These are scale factors commonly used for calculations of rare earth structures. They qualitatively reproduce the low observed levels of Er I very well. These calculations produced a transition rate of $\Gamma = 13$ s^{-1} for the 1299 nm line. This corresponds to a lifetime of 75 ms and an extremely narrow linewidth of 2.1 Hz. This long lifetime results from the fact that the 1299 nm level has more than 85% quintet character and thus does not combine well with the $4f^{12}6s^2\ ^3H_6$ ground state.

With such a long calculated lifetime, it was of interest to make sure that transitions to the lower level $4f^{11}(4I_{15/2}^o)5d_{5/2}6s^2(15/2, 5/2)_6^o$ by electric quadrupole or magnetic dipole radiation would not be comparable in rate with the calculated electric dipole rate. However, the calculated rates for the E2 and M1 transitions are much lower than the electric dipole rate for the transition to the ground state, so these transitions are not a factor for the present purpose.

To estimate the uncertainty of our calculated lifetime, we performed a series of calculations in which the scale factors were varied over large ranges. We found that the lifetime for 1299 nm was relatively insensitive to the scale factors for the internal interactions, but was highly sensitive to the scale factor for configuration interaction (CI). If we allow for an uncertainty of ± 0.10 in the CI scale factor, we obtain an uncertainty in the transition rate of ± 7 s^{-1} . Our value for the transition rate of the 1299 nm lines is thus 13 ± 7 s^{-1} .

Table 1. Laser cooling parameters for five transitions in Er.

Laser cooling parameter	Transition (listed by vacuum wavelength)				
	400.91 nm	582.84 nm	631.04 nm	841.22 nm	1299.21 nm
Γ	$1.7 \times 10^8 \text{ s}^{-1}$	$1.0 \times 10^6 \text{ s}^{-1}$	$1.8 \times 10^5 \text{ s}^{-1}$	$5.0 \times 10^4 \text{ s}^{-1}$	$13 \pm 7^c \text{ s}^{-1}$
τ	5.8 ns^a	$0.96 \text{ }\mu\text{s}^a$	$5.6 \pm 1.4 \text{ }\mu\text{s}^b$	$20 \pm 4 \text{ }\mu\text{s}^b$	75 ms
$\Delta\nu$	27 MHz	0.17 MHz	28 kHz	8.0 kHz	2.1 Hz
I_{sat}	560 W m^{-2}	1.1 W m^{-2}	0.15 W m^{-2}	18 mW m^{-2}	$1.3 \text{ }\mu\text{W m}^{-2}$
v_{capture}	11 m s^{-1}	0.97 m s^{-1}	18 mm s^{-1}	6.7 mm s^{-1}	$2.8 \text{ }\mu\text{m s}^{-1}$
T_{Doppler}	660 μK	4.0 μK	680 nK	190 nK	51 pK
v_{Doppler}	0.18 m s^{-1}	14 mm s^{-1}	5.8 mm s^{-1}	3.1 mm s^{-1}	$50 \text{ }\mu\text{m s}^{-1}$
T_{recoil}	350 nK	170 nK	140 nK	81 nK	34 nK
v_{recoil}	5.9 mm s^{-1}	4.1 mm s^{-1}	3.8 mm s^{-1}	2.8 mm s^{-1}	1.8 mm s^{-1}
^a Literature value [23] ^b Present work (experiment) ^c Present work (calculation)					

It should be mentioned that our calculation yields lifetimes for the 841 nm, 631 nm, 583 nm, and 401 nm levels of 22 μs , 4.5 μs , 0.61 μs , and 4.0 ns, respectively. These values are in fairly good agreement with the experimental values, suggesting that the calculation is capturing most of the essential physics for this atom.

7. Results

Table 1 summarizes the five $J \rightarrow J + 1$ laser cooling transitions that we have identified in Er. Using the present lifetime measurements for the 841 nm and 631 nm lines, the calculation for the 1299 nm line, and the literature values for the other transitions, we are able to fill out the table with relevant laser cooling parameters [22]. The saturation intensity $I_{\text{sat}} \equiv \pi \hbar c \Gamma / (3\lambda^3)$ is the laser intensity at which an ideal two-level atom would attain 25% excited state fraction, and is useful in determining what range of intensities are required for laser cooling. The capture velocity $v_{\text{capture}} \equiv \Gamma / k = \Gamma \lambda / 2\pi$ provides a measure for the velocity range over which atoms can be captured and cooled. The Doppler temperature $T_{\text{Doppler}} \equiv \hbar \Gamma / 2k_B$ and velocity $v_{\text{Doppler}} \equiv (k_B T_{\text{Doppler}} / m)^{1/2}$ describe the theoretical cooling limits attainable with Doppler cooling, and $T_{\text{recoil}} \equiv \hbar^2 k^2 / (2mk_B)$ and $v_{\text{recoil}} \equiv \hbar k / m$ describe similar limits for sub-Doppler cooling (m is the atomic mass and k_B is Boltzmann's constant).

Several interesting features of laser cooling in Er are evident from Table 1. On the 401 nm line, the capture velocity is quite large, making this a good transition for capturing atoms from a thermal source. At the same time, the recoil velocity for this transition is quite small. Significantly, the recoil velocity is smaller than the capture limit for the 841 nm line, suggesting the possibility of very efficient capture of atoms with the 401 nm line followed by transfer to cooling with the 841 nm line. Once atoms are trapped and cooled with the 841 nm line, attaining temperatures near the recoil limit of 80 nK with simple polarization gradient cooling becomes possible. This recoil temperature is much lower than that found in other narrowband-cooling atoms (the Ca limit is $\approx 3 \text{ }\mu\text{K}$ [11], the Sr limit is 230 nK, and the Yb limit is 180 nK), and hence record low laser cooling temperatures might be obtainable with Er.

Because the recoil velocity for the 1299 nm transition is larger than its capture velocity, simple laser cooling with this transition alone is not practical. Furthermore, the light force arising from scattering 1299 nm photons at a rate of 13 s^{-1} is several orders of magnitude smaller than gravity, making a magneto-optical trap unfeasible as well. Even if laser cooling is not performed on this line, though, it can be put to use for several interesting applications. Since the recoil velocity on this transition is smaller than the capture velocity for the 841 nm transition, it should be feasible to use this transition to interrogate atoms while they are simultaneously or periodically recooled on the 841 nm line. This suggests the possibility of high-accuracy atomic frequency standards that take advantage of the narrow linewidth of the 1299 nm transition. Furthermore, if the atoms are optically pumped into the stretched state with circularly polarized light, an effective two-level system can be attained with a long coherence time governed by the lifetime of the 1299 nm state. This fact, combined with the fact that the wavelength of this transition is in a low-loss, low-dispersion band for optical fiber communications, suggests possibilities for quantum cryptography and quantum information processing applications.

We have discussed new laser cooling opportunities for Er, and have presented new measurements and calculations of the lifetimes for three laser-accessible $J \rightarrow J+1$ transitions. Together with existing literature values for two other laser-accessible transitions, these lifetimes fill out an array of practical laser cooling opportunities spanning lifetimes from 5.8 ns to 75 ms and wavelengths from 401 nm to 1299 nm. Such a variety of laser cooling choices is not found in any other atom. Together with erbium's large ground-state magnetic moment and heavy mass, these choices should provide a wealth of opportunities for new laser cooling physics and applications.

Acknowledgments

The authors wish to thank members of the NIST Electron Physics Group for many useful technical discussions. We also thank J. V. Porto of the Laser Cooling Group for useful comments on the manuscript, and Yuri Ralchenko of the NIST Atomic Spectroscopy Group for assistance with the calculations. This material is based upon work supported in part by the National Science Foundation under Grant No. 0097450.